Schweizerischer Erdbebendienst
Service Sismologique Suisse
Servizio Sismico Svizzero
Servizi da Terratrembels Svizzer

ETH
Eidgenössische Technische Hochschule Zürich
Swiss Federal Institute of Technology Zurich

Grächen - Ausblick (SGRA)

SITE CHARACTERIZATION REPORT

Jan BURJANEK, Clotaire MICHEL, Gabriela GASSNER-STAMM

Valerio POGGI, Daniel ROTEN, Carlo CAUZZI, Donat FÄH

Sonneggstrasse 5 CH-8092 Zürich Switzerland; E-mail: clotaire.michel@sed.ethz.ch

Last modified : October 15, 2013

Abstract

Ambient vibration array measurements were performed in Graechen within the COGEAR and the Swiss Strong Motion Renewal projects. The measurements were adequate to characterize station SGRA of the Swiss Strong Motion Network, newly installed in 2010. The array used to estimate the velocity profile below the station has an aperture of $240\,\mathrm{m}$. The measurements were successful in deriving a velocity model for this site, which is a deep-seated landslide. The 20 first meters (moraine) are a gradient increasing from approximately 250 to $550\,\mathrm{m/s}$. At this depth, a sharp interface is found with velocities of the lower layer starting around $900\,\mathrm{m/s}$ and increasing with depth with a gradient-shape up to $2000\,\mathrm{m/s}$ at $400\,\mathrm{m}$ depth. Finally, the bedrock interface is found at $500\,\mathrm{m}$ but it is poorly constrained as well as the velocity in the bedrock. It corresponds to a fundamental resonance frequency of $0.7\,\mathrm{Hz}$. $V_{s,30}$ is found to be close to $580\,\mathrm{m/s}$. The EC8 and SIA261 ground types are B. Recordings on the new station will allow to validate the proposed 1D models.

Contents

1 Introduction

The station SGRA (Grächen Ausblick) is part of the Swiss Strong Motion Network (SSMNet) in the Valais region. SGRA was newly installed in the framework of the SSMNet Renewal project in 2010, densifying the SSMNet in the Valais in coordination with the COGEAR project. The SSMNet renewal project includes also the site characterization. The passive array measurement has been selected as a standard tool to investigate these sites. Several measurement campaigns were performed in Grächen in the frame of the COGEAR project [Burjánek et al., 2010]. Two are of particular interest to characterize the station site array GRA2 was performed 900 m away from station SGRA and array StN_array_3 $600\,\mathrm{m}$ away from the station. In addition, array GRA3 was performed $100\,\mathrm{m}$ away from station SGRA for both projects (Fig. 1). The station is located on debris of landslides and moraine and on a deep-seated landslide. This report presents the measurement setup of GRA3, the results of the array processing of the surface waves (dispersion curves). Comparison between the different experiments is presented. Then, an inversion of these results into velocity profiles is performed.

Canton	City	Location	Station code	Site type	Slope
Valais	Grächen	Ausblick	SGRA	Rock slope	$> 15\,^{\circ}$

Table 1: Main characteristics of the study-site.

Figure 1: Picture of the GRA3 array.

2 Experiment description (GRA3)

2.1 Ambient Vibrations

The ground surface is permanently subjected to ambient vibrations due to:

- natural sources (ocean and large-scale atmospheric phenomena) below $1\,\mathrm{Hz}$,
- local meteorological conditions (wind and rain) at frequencies around $1\,\mathrm{Hz}$,
- human activities (industrial machines, traffic…) at frequencies above $1\,\mathrm{Hz}$ [Bonnefoy-Claudet et al., 2006].

The objective of the measurements is to record these ambient vibrations and to use their propagation properties to infer the underground structure. First, the polarization of the recorded waves (H/V ratio) are used to derive the resonance frequencies of the ground layers. Second, the phase delays between stations are used to derive the velocity of surface waves at different frequencies (dispersion). The information (H/V, dispersion curves) is then used to derive the properties of the soil layers using an inversion process.

2.2 Equipment

For these measurements 12 Quanterra Q330 dataloggers named NR1 to NR12 and 14 Lennartz 3C 5 s seismometers were available (see Tab. 2). Each datalogger can record on 2 ports A (channels EH1, EH2, EH3 for Z, N, E directions) and B (channels EH4, EH5, EH6 for Z, N, E directions). The time synchronization was ensured by GPS. The sensor are placed on a metal tripod in a $20\,\mathrm{cm}$ hole, when possible, for a better coupling with the ground.

Digitizer	**Model**	**Number**	**Resolution**
	Quanterra Q330	12	$24\,\mathrm{bits}$
Sensor type	**Model**	**Number**	**Cut-off frequency**
Velocimeter	Lennartz 3C	14	$0.2\,\mathrm{Hz}$

Table 2: Equipment used.

2.3 Geometry of the array

Two array configurations were used, for a total of 4 rings of 10, 25, 60 and $120\,\mathrm{m}$ radius around a central station. The first configuration includes the 3 inner rings with 13 sensors (point GRA301 was not recorded); the second configuration includes the 2 outer rings with 10 sensors. The minimum inter-station distance and the aperture are therefore 10 and $120\,\mathrm{m}$ and 60 and $240\,\mathrm{m}$, respectively. The experimental setup is displayed in Fig. 2. The final usable datasets are detailed in section 3.2.

Figure 2: Geometry of the arrays.

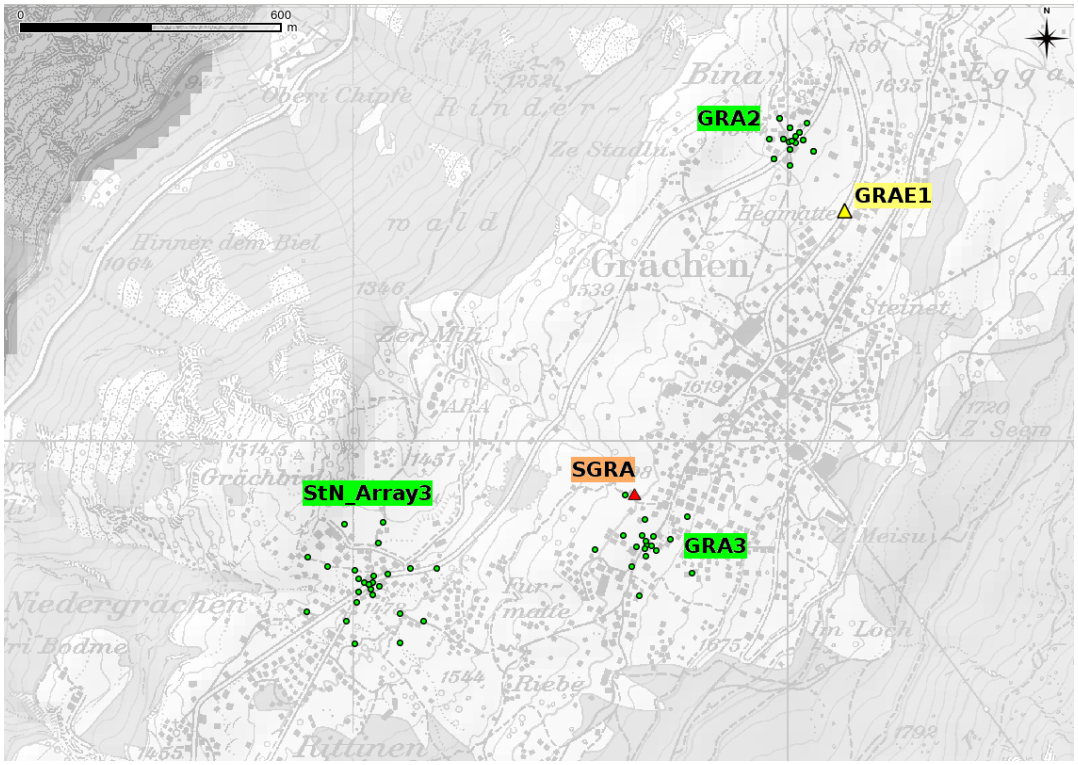

Figure 3: An overview of array measurements at Graechen. Red triangle represents the new strong motion station SGRA.

2.4 Positioning of the stations

The sensor coordinates were measured using a differential GPS device (Novatel), including a base station and a rover station. The differential GPS computation is done by post-processing using the GraphNav software.

3 Data quality

3.1 Usable data

The largest time windows were extracted, for which all the sensors of the array were in position and the GPS synchronization was ensured. Station NR8 (point GRA301) did not record. The characteristics of the datasets are detailed in Tab. 3.

3.2 Data processing

The data from the Quanterra stations were first converted to SAC format, including in the header the sensor coordinates (CH1903 system), the recording component and a name related to the position of the station. The name is made of 3 letters characterizing the location (GRA here) and 3 digits. Recordings were not corrected from the instrument response.

Dataset	Starting Date	Time	Length	F_s	Min. inter-distance	Aperture	# of points
1	2010/07/08	8:55	95 min	200 Hz	10 m	120 m	13
2	2010/07/08	11:30	65 min	200 Hz	60 m	240 m	10

Table 3: Usable datasets.

4 Array processing

4.1 Methods

Different methods and algorithms were tested and compared.

The first array method we used is based on the high-resolution beam-forming (HRBF). It was originally proposed by Capon [1969] but developed and applied to vertical recordings of ambient vibrations by Kind et al. [2005]. We have extended this method to analyze also the horizontal components [Fäh et al., 2008]. Ambient noise consists mostly of surface-waves, and surface-waves are dispersive. This means that wave-packages with different frequency content are propagating with different velocities. In general, subarrays with different apertures are set up for the measurement to optimize the resolution in a certain frequency band. Small apertures are used to resolve the shallow part of a structure, and by increasing the aperture, deeper and deeper structures can be investigated. The final dispersion curve over a wide frequency range is then composed of the parts obtained by the different subarrays. The limits of each subarray are given by the aliasing at high frequencies and the loss of resolution at low frequencies.

Ellipticity of Rayleigh waves was shown to be useful additional constrain for the inversion of dispersion curves [Fäh et al., 2003]. The estimate of ellipticity by f-k method (array method) was introduced by Poggi and Fäh [2010]. It is based on the assumption that a peak in the f-k cross-spectrum obtained from horizontal (radial-polarized) and vertical components of motion must be representative of the signal power of a particular Rayleigh wave mode. Thus the relative frequency-dependent surface displacement ratio can be calculated for each mode separately, once the mode-correspondent dispersion curve is identified on the f-k plane.

In the wavelet-based method of ellipticity estimation, the time-frequency representations of the vertical and both horizontal components are computed using continuous wavelet transform (CWT). In contrast to Love waves, Rayleigh waves will have an energy maximum on the vertical component. Therefore, to extract mostly Rayleigh waves, the absolute value of the CWT for the vertical component is scanned for all maxima. For each maximum identified on the time axis, the value of horizontal component wavelet coefficient is picked with a delay of one quarter of period. That is the theoretical delay between vertical and horizontal components for a Rayleigh wave. It can be positive (prograde particle motion) or negative (retrograde particle motion). The ratio between horizontal and vertical values is saved for each maximum found on the vertical component. Ratios are analyzed statistically, and the whole process is repeated for all frequencies, so the ellipticity of fundamental Rayleigh wave is estimated. We apply a method that was developed during the European project NERIES (Network of Research Infrastructures for European Seismology) joint research activity JRA4 [Fäh et al., 2009].

4.2 Results

FK processing results in quite peculiar result for this array (Fig. 4). Picked Love dispersion curve follows Rayleigh dispersion curve. Since other two array measurements were performed close by (see Fig. 3), joint interpretation of dispersion curve might bring more insight (see Fig. 4). The Rayleigh dispersion curves present good agreement among the three arrays. In particular, the three curves converge to the same low frequency and high frequency asymptotes.

Therefore we conclude that subsurface composition is very similar at the three sites, just the depths of the interfaces are likely changing. In case of Love waves, we obtained just band limited dispersion curves for StN_Array3 and GRA2, however, they are very well separated from the Rayleigh DC. This is not the case of the GRA3 array, where the picks at transversal component are very close to the Rayleigh wave DC. Assuming qualitative match of DC for the three arrays (as in case of Rayleigh DC) we find the pick from the transversal component of the GRA3 array unreliable, and we do not use it in the inversion.

The H/V curve computed at each array point and compared to the ellipticity extracted from the 3C FK analysis [Poggi and Fäh, 2010] is presented on Fig. 5. They all show a fundamental frequency peak at $0.7\,\mathrm{Hz}$.

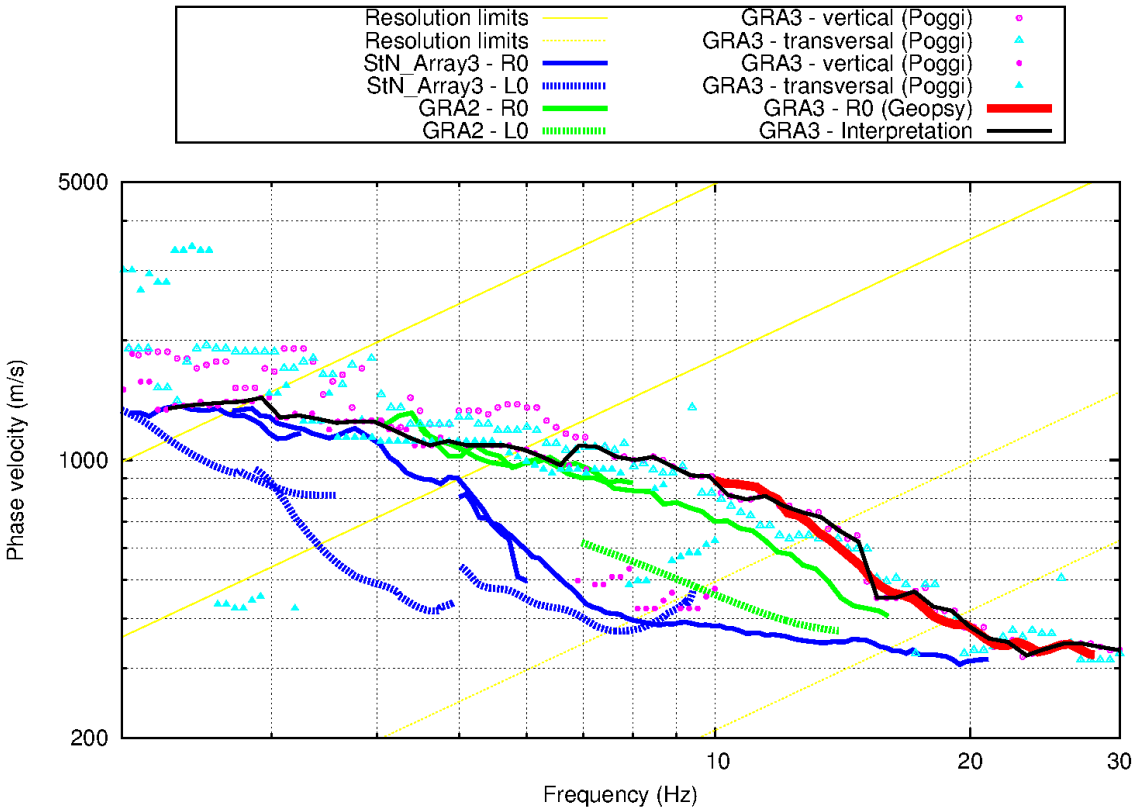

Figure 4: A complete set of dispersion curves (DC) for Graechen area

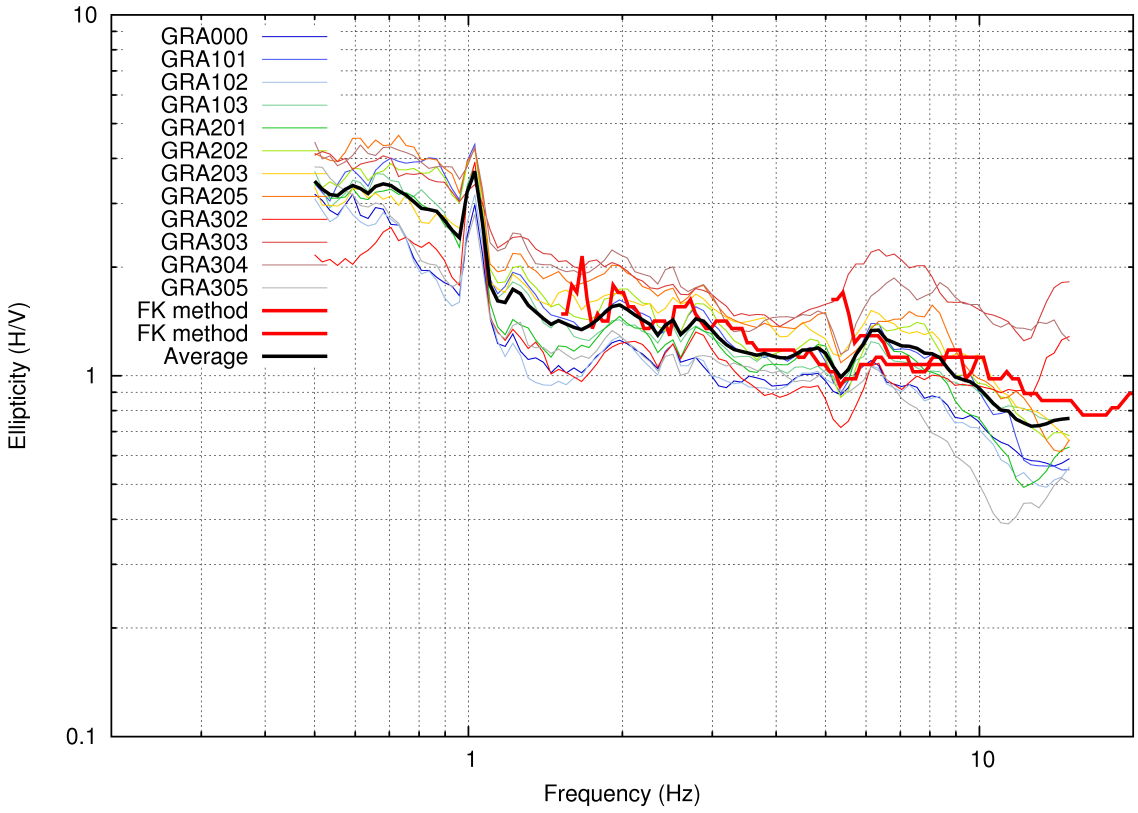

Figure 5: A complete set of ellipticity curves (H/V) for the array

5 Inversion and interpretation

5.1 Inversion

For the inversion we used "dinver", implemented within the GEOPSY software package (`http://www.geopsy.org`). Dinver is using the Conditional Neighbourhood Algorithm for solving inversion problems [Wathelet, 2008].

A number of joint inversions (Rayleigh DC + ellipticity) was performed (see Fig. 6). It was hard to fit both DC and ellipticity, thus we tested several different values of the relative weights (see different rows in Fig. 6). The results are also compared with GRA2 inversion results (Fig. 6, bottom row). In general, the results are similar – rapid increase of the shear wave velocity in the first 20 meters (from 300 to 900 m/s), followed by weak gradient (1000 to 2000m/s) down to 300-400m, and a stronger gradient (potential interface) around the depth of 400m, which is constrained by the peak in the ellipticity. The GRA3 Rayleigh DC favors slightly faster middle part of the profile (20-300m), which pushes the deep interface even deeper (>500m). On the other hand, putting more weight on the ellipticity brings the results closer to the GRA2 results, which are quite well constrained (good fit for all Rayleigh, Love DC and Rayleigh ellipticity – see Fig. 6). To conclude, the uncertainty of the results for the GRA3 array is quite large compared to the other two arrays in the area. The final selection of the representative models covers best 10 models of each inversion (first four rows in Fig. 6), so that 40 models in total.

Velocity down to $200\,\mathrm{m}$ remains below $1500\,\mathrm{m/s}$, which is particularly low for rock, and increases gradually but significantly below this depth. This has to be interpreted in the light of the deep-seated landslide that has its basement at $200-300\,\mathrm{m}$ depth in Grächen according to the geologists [Eichenberger et al., 2010]. Even if the depth of this basement cannot be precisely seen with the data presented here, it confirms this interpretation.

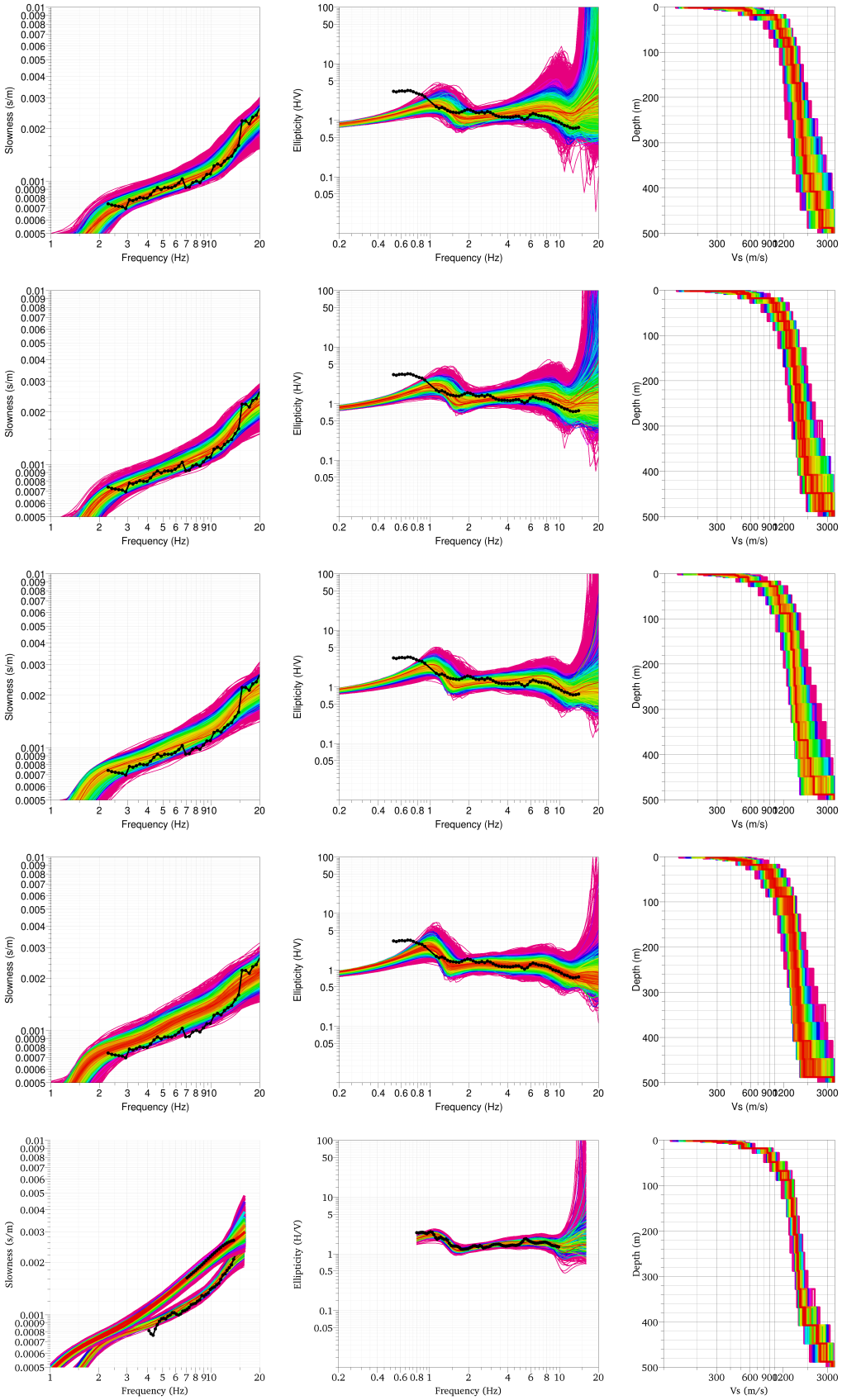

Figure 6: Inversion for the GRA3 array (first four rows), changing the relative weight of the ellipticity. Results for GRA2 are shown in the last row for a comparison.

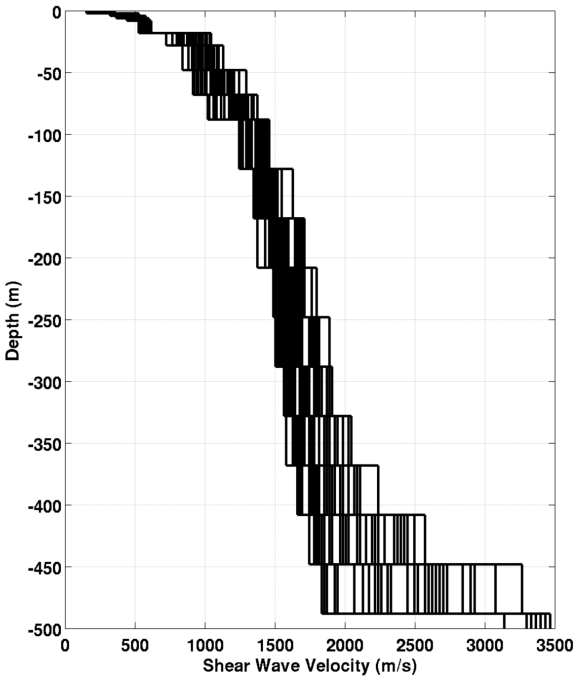

Figure 7: V_s ground profiles for the selected 40 best models.

5.2 Travel time average velocities and ground type

The distribution of the travel time average velocities at different depths was computed from the selected models. The uncertainty, computed as the standard deviation of the distribution of travel time average velocities for the considered models, is also provided, but its meaning is doubtful since the parameter space was not fully explored. $V_{s,30}$ is found to be $576\,\mathrm{m/s}$, that is associated to type B in the Eurocode 8 [CEN, 2004] and SIA261 [SIA, 2003].

	Mean (m/s)	**Uncertainty (m/s)**
$V_{s,5}$	322	32
$V_{s,10}$	398	22
$V_{s,20}$	485	17
$V_{s,30}$	576	19
$V_{s,40}$	644	22
$V_{s,50}$	694	25
$V_{s,100}$	878	38
$V_{s,150}$	1002	37
$V_{s,200}$	1094	39

Table 4: Travel time averages at different depths from the inverted models. Uncertainty is given as one standard deviation from the selected profiles.

5.3 SH transfer function and quarter-wavelength velocity

The quarter-wavelength velocity approach [Joyner et al., 1981] provides, for a given frequency, the average velocity at a depth corresponding to 1/4 of the wavelength of interest. It is useful to identify the frequency limits of the experimental data (minimum frequency in dispersion curves at $2.3\,\mathrm{Hz}$ and in the ellipticity curve $0.6\,\mathrm{Hz}$ here). The results using this proxy show that the dispersion curves constrain the profiles down to $90\,\mathrm{m}$ and the ellipticity data down to $700\,\mathrm{m}$ (Fig. 8). Moreover, the quarter wavelength impedance-contrast introduced by Poggi et al. [2012] is also displayed in the figure. It corresponds to the ratio between two quarter-wavelength average velocities, respectively from the top and the bottom part of the velocity profile, at a given frequency [Poggi et al., 2012]. It shows a trough (inverse shows a peak) at the resonance frequency.

Moreover, the theoretical SH-wave transfer function for vertical propagation [Roesset, 1970] is computed from the inverted profiles. It is compared to the quarter-wavelength amplification [Joyner et al., 1981], that however cannot take resonances into account (Fig. 9). In this case, the models are predicting an increasing amplification with frequency with small amplification peaks at the resonance frequencies (1 and $2.5\,\mathrm{Hz}$).

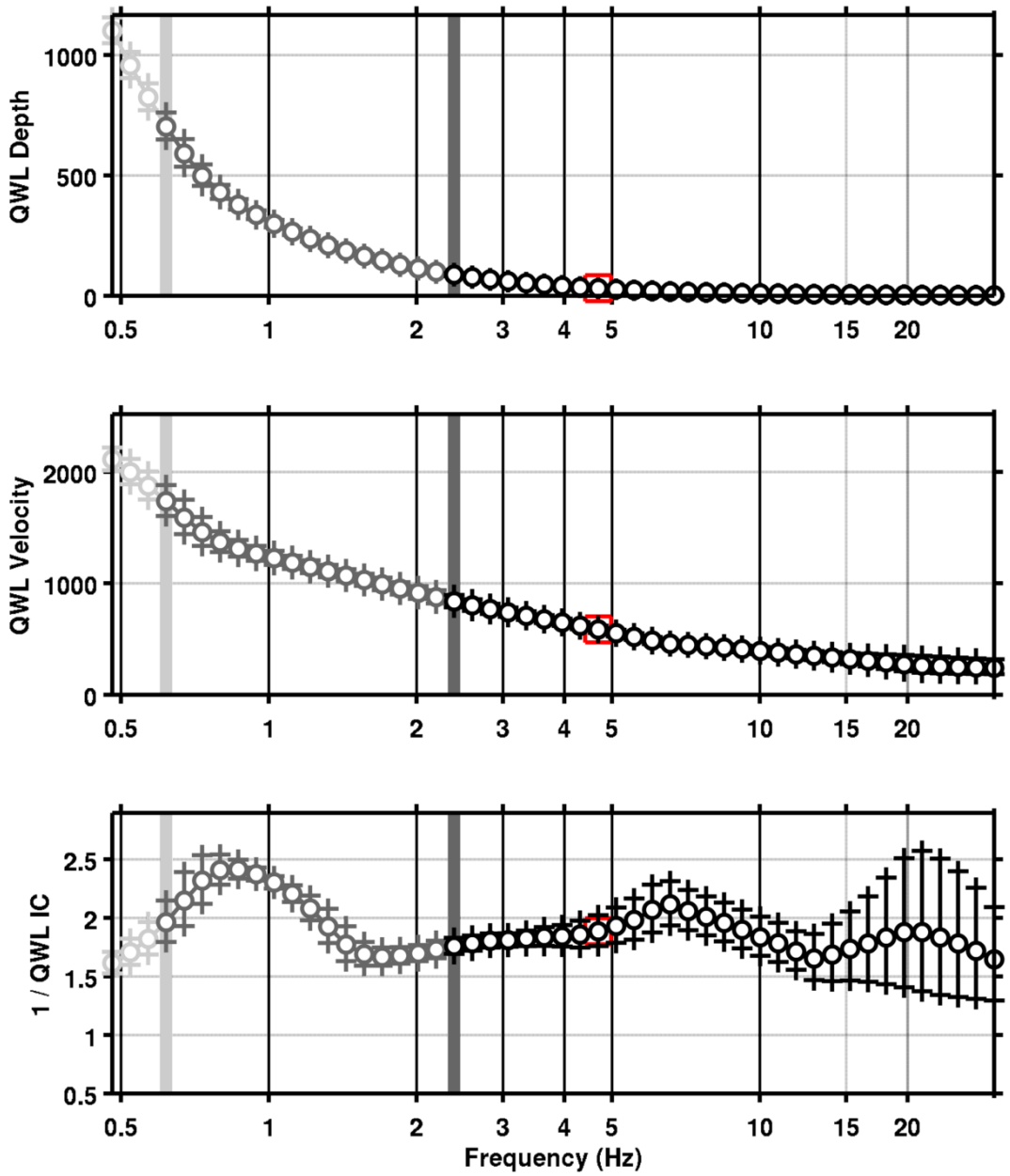

Figure 8: Quarter wavelength velocity representation of the velocity profile (top: depth, centre: velocity, bottom: inverse of the impedance contrast). Black curve is constrained by the dispersion curves, light grey is not constrained by the data. Red square is corresponding to $V_{s,30}$.

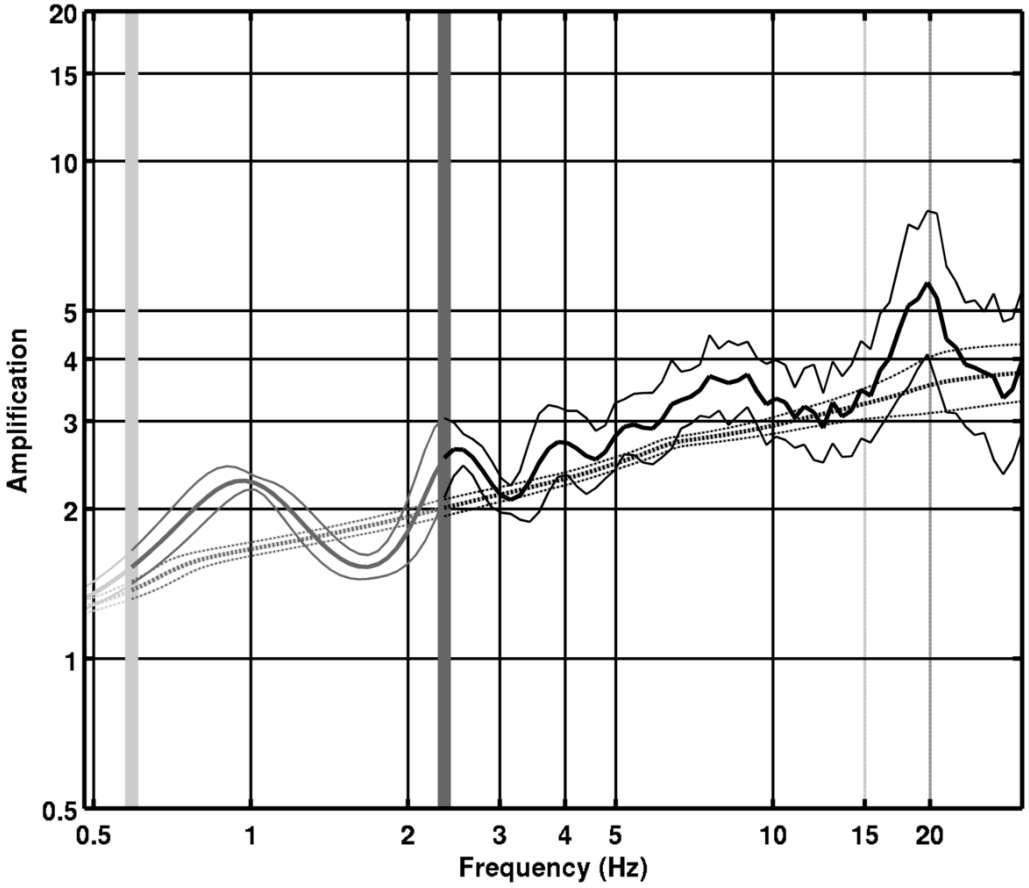

Figure 9: Theoretical SH transfer function (solid line) and quarter wavelength impedance contrast (dashed line) with their standard deviation. Significance of the greyshades is detailed in Fig. 8.

6 Conclusions

The array measurements in Graechen were successful in deriving a velocity model for the site of the strong motion station SGRA. We found a gradient velocity profile with some sharp interfaces. The 20 first meters are a gradient increasing from approximately 250 to $550\,\mathrm{m/s}$ made of moraine according to Dupray et al. [2012]. At this depth, a sharp interface is found with velocities of the lower layer starting around $900\,\mathrm{m/s}$ and increasing with depth with a gradient-shape up to $2000\,\mathrm{m/s}$ at $400\,\mathrm{m}$ depth. Finally, the bedrock interface is found at $500\,\mathrm{m}$ but it is poorly constrained as well as the velocity in the bedrock. It corresponds to a fundamental resonance frequency of $0.7\,\mathrm{Hz}$. $V_{s,30}$ is found to be close to $580\,\mathrm{m/s}$. The EC8 and SIA261 ground types are B. Recordings on the new station will allow to validate the proposed 1D models.

References

Sylvette Bonnefoy-Claudet, Fabrice Cotton, and Pierre-Yves Bard. The nature of noise wavefield and its applications for site effects studies. *Earth-Science Reviews*, 79(3-4): 205–227, December 2006. ISSN 00128252. doi: 10.1016/j.earscirev.2006.07.004. URL http://linkinghub.elsevier.com/retrieve/pii/S0012825206001012.

Jan Burjánek, Gabriela Gassner-Stamm, and Donat Fäh. COGEAR Module 3: Array measurements in the area of Visp and St. Niklaus. Technical report, Swiss Seismological Service, ETH Zürich, Zürich, 2010.

J. Capon. High-Resolution Frequency-Wavenumber Spectrum Analysis. *Proceedings of the IEEE*, 57(8):1408–1418, 1969.

CEN. *Eurocode 8: Design of structures for earthquake resistance - Part 1: General rules, seismic actions and rules for buildings*. European Committee for Standardization, en 1998-1: edition, 2004.

F. Dupray, L Chao, A Seiphoori, and L. Laloui. COGEAR Module 3: Modelling of slope behaviour and nonlinear phenomena - 1D non-linear simulations for a case study in Grächen. Technical report, EPFL, Lausanne, Switzerland, 2012.

John Eichenberger, A. Ferrari, C. Schurmann, and L. Laloui. COGEAR Module 3: Overview of existing data in the Matter valley (soil slopes). Technical report, Laboratory of Soil Mechanics, EPFL, Lausanne, Switzerland, 2010.

Donat Fäh, Fortunat Kind, and Domenico Giardini. Inversion of local S-wave velocity structures from average H/V ratios, and their use for the estimation of site-effects. *Journal of Seismology*, 7(4):449–467, October 2003. ISSN 1383-4649. doi: 10.1023/B:JOSE.0000005712.86058.42. URL http://link.springer.com/10.1023/B:JOSE.0000005712.86058.42.

Donat Fäh, Gabriela Stamm, and Hans-Balder Havenith. Analysis of three-component ambient vibration array measurements. *Geophysical Journal International*, 172(1):199–213, January 2008. ISSN 0956540X. doi: 10.1111/j.1365-246X.2007.03625.x. URL http://doi.wiley.com/10.1111/j.1365-246X.2007.03625.x.

Donat Fäh, Marc Wathelet, Miriam Kristekova, Hans-Balder Havenith, Brigitte Endrun, Gabriela Stamm, Valerio Poggi, Jan Burjanek, and Cécile Cornou. Using Ellipticity Information for Site Characterisation Using Ellipticity Information for Site Characterisation. Technical report, NERIES JRA4 Task B2, 2009.

William B. Joyner, Richard E. Warrick, and Thomas E. Fumal. The effect of Quaternary alluvium on strong ground motion in the Coyote Lake, California, earthquake of 1979. *Bulletin of the Seismological Society of America*, 71(4):1333–1349, 1981.

Fortunat Kind, Donat Fäh, and Domenico Giardini. Array measurements of S-wave velocities from ambient vibrations. *Geophysical Journal International*, 160(1):114–126, December 2005. ISSN 0956540X. doi: 10.1111/j.1365-246X.2005.02331.x. URL http://gji.oxfordjournals.org/cgi/doi/10.1111/j.1365-246X.2005.02331.x.

Valerio Poggi and Donat Fäh. Estimating Rayleigh wave particle motion from three-component array analysis of ambient vibrations. *Geophysical Journal International*, 180(1):251–267, January 2010. ISSN 0956540X. doi: 10.1111/j.1365-246X.2009.04402.x. URL http://doi.wiley.com/10.1111/j.1365-246X.2009.04402.x.

Valerio Poggi, Benjamin Edwards, and Donat Fäh. Characterizing the Vertical-to-Horizontal Ratio of Ground Motion at Soft Sediment-Sites. *Bulletin of the Seismological Society of America*, 102(6), 2012. doi: 10.1785/0120120039.

J.M. Roesset. Fundamentals of soil amplification. In R. J. Hansen, editor, *Seismic Design for Nuclear Power Plants*, pages 183–244. M.I.T. Press, Cambridge, Mass., 1970. ISBN 978-0-262-08041-5. URL http://mitpress.mit.edu/catalog/item/default.asp?ttype=2\&tid=5998.

SIA. *SIA 261 Actions sur les structures porteuses*. Société suisse des ingénieurs et des architectes, Zürich, sia 261:20 edition, 2003.

Marc Wathelet. An improved neighborhood algorithm: Parameter conditions and dynamic scaling. *Geophysical Research Letters*, 35(9):1–5, May 2008. ISSN 0094-8276. doi: 10.1029/2008GL033256. URL http://www.agu.org/pubs/crossref/2008/2008GL033256.shtml.